nature immunology

Early window of diabetes determinism in NOD mice, dependent on the complement receptor CRIg, identified by noninvasive imaging

Wenxian Fu[1], Gregory Wojtkiewicz[2,3], Ralph Weissleder[2–4], Christophe Benoist[1,4] & Diane Mathis[1,4,5]

All juvenile mice of the nonobese diabetic (NOD) strain develop insulitis, but there is considerable variation in their progression to diabetes. Here we used a strategy based on magnetic resonance imaging (MRI) of magnetic nanoparticles to noninvasively visualize local effects of pancreatic-islet inflammation to predict the onset of diabetes in NOD mice. MRI signals acquired during a narrow early time window allowed us to sort mice into groups that would progress to clinical disease or not and to estimate the time to diabetes development. We exploited this approach to identify previously unknown molecular and cellular elements correlated with disease protection, including the complement receptor of the immunoglobulin superfamily (CRIg), which marked a subset of macrophages associated with diabetes resistance. Administration of a fusion of CRIg and the Fc portion of immunoglobulin resulted in lower MRI signals and diabetes incidence. In addition to identifying regulators of disease progression, we show here that diabetes is set at an early age in NOD mice.

Type 1 diabetes is an organ-specific autoimmune disease characterized by specific destruction of the insulin-producing beta cells of the pancreatic islets of Langerhans[1]. Autoimmune diabetes is driven mainly by T lymphocytes that respond to beta cell–specific antigens, but other cells of the immune system can also have an important enhancing or dampening role, notably B lymphocytes, natural killer cells, macrophages and dendritic cells (DCs). This disease has two main checkpoints in most mouse models: initiation of insulitis at 2–5 weeks of age; and, with a highly variable delay and penetrance, conversion of insulitis to overt diabetes[2]. Whether these same two checkpoints exist in human type 1 diabetes has been the subject of discussion, but there have been indications that they do.

The issues noted above and others underscore the relative ignorance about the pathogenesis of autoimmune diabetes, particularly in humans. A major hindrance in both experimental and clinical contexts has been the inability to directly visualize the onset and progression of islet attack. Experimentally, investigators are constantly challenged by the scatter in disease parameters of individual animals, even those presumed to be genetically and environmentally homogeneous. For example, a particular 15-week-old mouse of the nonobese diabetic (NOD) strain with advanced insulitis may develop clinical diabetes in days, weeks or months, or never. Clinically, beyond the same problem of disease heterogeneity, a diagnosis of overt diabetes generally indicates that most of a patient's beta cells have already been destroyed or disabled, which means that the early, autoimmune phases of the process have already ended and that strategies for disease reversal are limited.

In recognition of the impediments noted above, much effort has been devoted to the identification of biomarkers that indirectly signal at least the major landmarks of the pathogenesis of type 1 diabetes. So far, serum autoantibody titers seem to be the best indicators of islet attack, which was confirmed in the Diabetes Prevention Trial-Type 1 (ref. 3). The appearance of autoantibody specificities to at least one beta-cell antigen is generally considered to reflect insulitis; the emergence of specificities to two or more can be used to predict the eventual conversion of insulitis to diabetes. Plasma C-peptide concentrations are still the most widely accepted indicator of beta-cell activity. C peptide is secreted in concentrations equimolar to those of insulin and is a semiquantitative marker of beta-cell secretion that is not subject to hepatic extraction, in contrast to insulin[4]. Although monitoring autoantibody titers and C-peptide concentrations certainly provides useful information, a noninvasive means of more directly monitoring disease progression would have several important experimental and clinical applications. There are two fundamental needs: an assessment of islet infiltration, as a 'read-out' of ongoing autoimmune attack; and quantification of beta-cell mass or function, as an indicator of cumulative islet destruction. Although substantial effort has been expended to address these goals, no clinically reliable method is now in place[5].

A noninvasive, real-time, whole-mouse imaging method has been successfully used for visualizing vascular and inflammatory-cell changes that signal disease checkpoints in mouse models of type 1 diabetes[6,7]. Insulitis is essentially an inflammation of the pancreatic

[1]Division of Immunology, Department of Microbiology and Immunobiology, Harvard Medical School, Boston, Massachusetts, USA. [2]Systems Biology, Harvard Medical School, Boston, Massachusetts, USA. [3]Center for Systems Biology, Massachusetts General Hospital, Boston, Massachusetts, USA. [4]Broad Institute of MIT and Harvard, Cambridge, Massachusetts, USA. [5]Harvard Stem Cell Institute, Cambridge, Massachusetts, USA. Correspondence should be addressed to C.B. (cbdm@hms.harvard.edu) or D.M. (cbdm@hms.harvard.edu).

Received 19 September 2011; accepted 11 January 2012; published online 26 February 2012; doi:10.1038/ni.2233

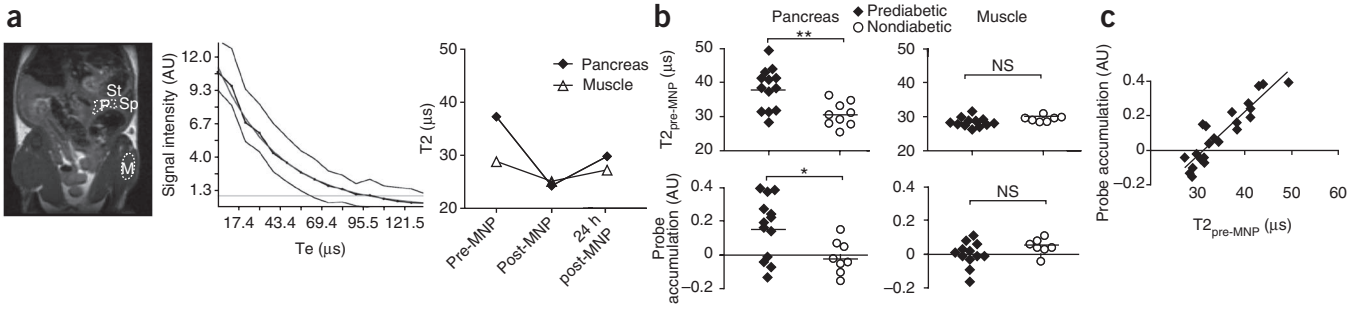

Figure 1 Prediction of type 1 diabetes in NOD mice by MRI-MNP: a cross-sectional cohort. (**a**) MNP-MRI methodology. Left, T2-weighted whole-mouse MRI image (coronal view). M, muscle; P, pancreas; Sp, spleen; St, stomach. Middle, calculation of T2 values (as described in Online Methods). Te, echo time; AU, arbitrary units. Right, T2 values for pancreas and muscle at the three standard time points: before (pre-MNP), immediately after (post-MNP) and 24 h after (24 h post-MNP) injection of MNPs (horizontal axis). (**b**) T2 values before injection of MNPs ($T2_{pre-MNP}$; top) and probe accumulation (below) for female NOD mice 10–17 weeks of age ($n = 22$) given injection of MNPs, followed by MRI scans of the pancreas and muscle (as in **a**); mice were monitored until 40 weeks, which permitted retroactive assignment into groups that did (prediabetic) or did not (nondiabetic) develop clinical diabetes. Each symbol represents an individual mouse; small horizontal lines indicate the mean. NS, not significant. $^*P = 0.02$ and $^{**}P = 0.0023$ (Student's *t*-test.). (**c**) Correlation between baseline T2 and probe-accumulation values of the mice in **b**. μs, microsecond. $R^2 = 0.8397$; $P < 0.0001$ (F-test). Data are representative of three experiments (**a**) or are combined from three experiments (**b**,**c**).

islets and thus is accompanied by a range of microvascular alterations, including modifications of endothelial cells, vascular swelling and leakage, more islet blood flow and edema[8–10], as well as by influxes of inflammatory-cell populations, in particular early infiltration of macrophages[11]. A new method that entails magnetic resonance imaging (MRI) of magnetic nanoparticles (MNPs) is sensitive to such changes, permitting monitoring of disease progression, quantification of genetically determined variability in disease, signaling of the imminent onset of diabetes and a very early indication of immunotherapy-induced disease reversal[6,7]. Notably, a small clinical trial of patients with recent-onset type 1 diabetes has confirmed the utility of this MRI-MNP approach in the human context[12].

Here we exploited the MRI-MNP strategy as a prediction tool in the NOD mouse model of type 1 diabetes. Unexpectedly, optimum predictability occurred during a narrow time window between 6 and 10 weeks of age, long before the eventual conversion of insulitis to overt diabetes. Use of this approach to sort 6- to 10-week-old insulitic mice that should or should not go on to develop diabetes permitted us to identify molecules and cells associated with aggressive versus innocuous insulitis, which identified a novel pathway important in regulating diabetes progression.

RESULTS

Predicting the conversion of insulitis to diabetes

All mice in our NOD mouse colony, regardless of their sex, develop insulitis starting at about 3–5 weeks after birth. However, overt diabetes develops in only 60–80% of female mice and 10–20% of male mice, any time from 15 to 30 weeks of age. This heterogeneity in disease penetrance and kinetics compromises the accuracy of mechanistic explorations because we do not know for a given individual mouse if and when it will eventually convert to diabetes. Thus, we set out to develop a noninvasive method to predict diabetes onset in mouse models.

The published MRI-MNP technique tracks a long-circulating, dextran-coated, monocrystalline, super-paramagnetic, iron-oxide probe (MION-47) that can be detected by high-resolution MRI[6,7]. Building on those past studies, the basic protocol for our experiments was to anesthetize groups of mice and obtain an MRI scan before injection of MNPs (baseline signal); to inject them intravenously with MNPs and immediately obtain a second image (an indicator of vascular volume); and to do a third scan 24 h later (a reflection of probe accumulation). We drew regions of interest over the pancreas and control muscle tissue on the MRI scan (**Fig. 1a**, left) and calaculated a value for the spin-spin relaxation time (T2 value) for each organ (**Fig. 1a**, middle); organ T2 values are diminished in the presence of MNPs. We determined probe-accumulation values, a function of vascular leakage and macrophage uptake[7], using the reciprocal of the T2 values before and 24 h after injection of MNPs (**Fig. 1a**, right).

We used both cross-sectional and longitudinal imaging designs. For the cross-sectional protocol, we injected 22 NOD female mice ranging from 10 to 17 weeks of age with MNPs, triple-scanned pancreata and control muscles as described above and monitored the mice for signs of diabetes until 40 weeks of age. We retrospectively assigned mice to two groups: those that eventually developed diabetes ($n = 13$; called 'prediabetic' here) and those that did not ($n = 9$; called 'nondiabetic' here). We determined pancreas and muscle T2 signals for individual mice (**Supplementary Fig. 1**) and plotted the corresponding baseline T2 values (before injection of MNPs) and probe-accumulation values (**Fig. 1b**). Two main differences between prediabetic and nondiabetic mice were evident. First, the baseline T2 signals were higher for the pancreas, but not muscle, of mice that went on to develop diabetes (**Fig. 1b**, top), which suggested the existence of edema measurable by MRI even in the absence of MNPs. Second, probe accumulation was also greater for the pancreas of prediabetic mice than for that of nondiabetic mice, but this observation was not true for muscle (**Fig. 1b**, bottom). There was a significant correlation between the pancreatic T2 values (before injection of MNPs) and probe-accumulation values across the whole cohort (**Fig. 1c**).

Next we addressed how early in the course of the NOD disease this MRI-MNP approach could be used to predict the eventual onset of diabetes. For this longitudinal design, we sequentially scanned synchronous cohorts of juvenile mice every 3–4 weeks until 18 weeks of age (**Fig. 2**), an interval known to be adequate for probe washout[13]. We monitored mice for signs of diabetes until they were 40 weeks old, which permitted retrospective assignment into the nondiabetes and prediabetes groups and, for the latter, calculation of time to diabetes. Unexpectedly, the MRI-MNP signals of 6- and 10-week-old mice were the most predictive (**Fig. 2a**,**b**), especially probe-accumulation values at 10 weeks, which essentially did not overlap for nondiabetic and prediabetic mice (**Fig. 2b**). Plots of probe-accumulation and blood-glucose values for individual mice over time solidified that observation (**Supplementary Fig. 2a**). There was also significant correlation

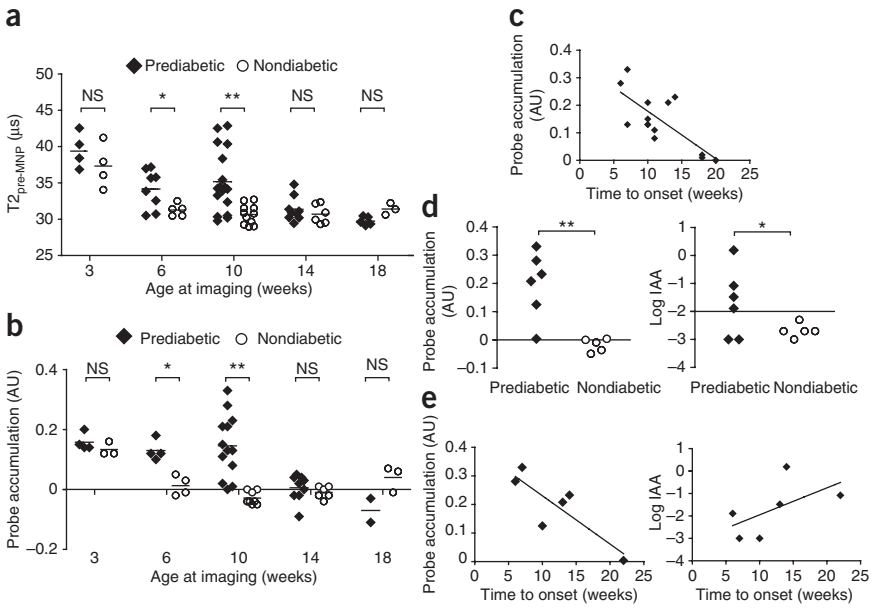

Figure 2 Prediction of type 1 diabetes in NOD mice: longitudinal cohorts. (**a**) Pancreatic T2 values before MNP injection in cohorts of 3-week-old female NOD mice, which were given injection of MNPs and imaged (as in **Fig. 1**), then reinjected and reimaged every 3–4 weeks until 18 weeks of age; mice were monitored for 40 weeks for assignment as prediabetic or nondiabetic (as in **Fig. 1b**). $*P = 0.0194$ and $**P = 0.0006$ (Student's *t*-test). (**b**) Pancreatic probe-accumulation values of the mice in **a**. $*P = 0.0037$ and $**P = 0.0001$ (Student's *t*-test). (**c**) Correlation between pancreatic probe-accumulation values at 10 weeks and time to onset of diabetes for the mice in **a** ($n = 13$). $R^2 = 0.5557$; $P = 0.0034$ (F-test). (**d**,**e**) Comparison of success of MNP-MRI (left) and autoantibody to insulin (IAA; right) in the prediction of type 1 diabetes in 10-week-old mice (monitored until 40 weeks of age). (**d**) Values for individual mice at 10 weeks. $*P = 0.1167$ and $**P = 0.0031$ (Student's *t*-test). (**e**) Correlation between values at 10 weeks and time to diabetes onset. Left, $R^2 = 0.7073$; $P = 0.0359$ (F-test). Right, $R^2 = 0.3301$; $P = 0.0645$ (F-test). Each symbol (**a**–**e**) represents an individual mouse; small horizontal lines (**a**,**b**) indicate the group mean. Data are combined from five experiments (**a**–**c**) or two experiments with 11 mice (**d**,**e**).

between the amount of probe accumulation and the time to diabetes onset (**Fig. 2c**). After 10 weeks, mice of either disease status showed relatively low baseline T2 and probe-accumulation values, consistent with published observations[6]. Before 6 weeks, both nondiabetic and prediabetic mice had relatively high values, which probably reflected the immature condition of the vasculature, with incomplete closure of endothelial cell junctions[14]. High pancreatic MRI signals at this time point did not reflect insulitis, as we obtained similar values for 3-week-old Eα16/NOD mice, which lack both insulitis and diabetes[15] (**Supplementary Fig. 2b**). The signals were also not a specific feature of the NOD strain, as C57BL/6 mice had similar values at this young age (**Supplementary Fig. 2b**). In both Eα16/NOD and C57BL/6 mice,

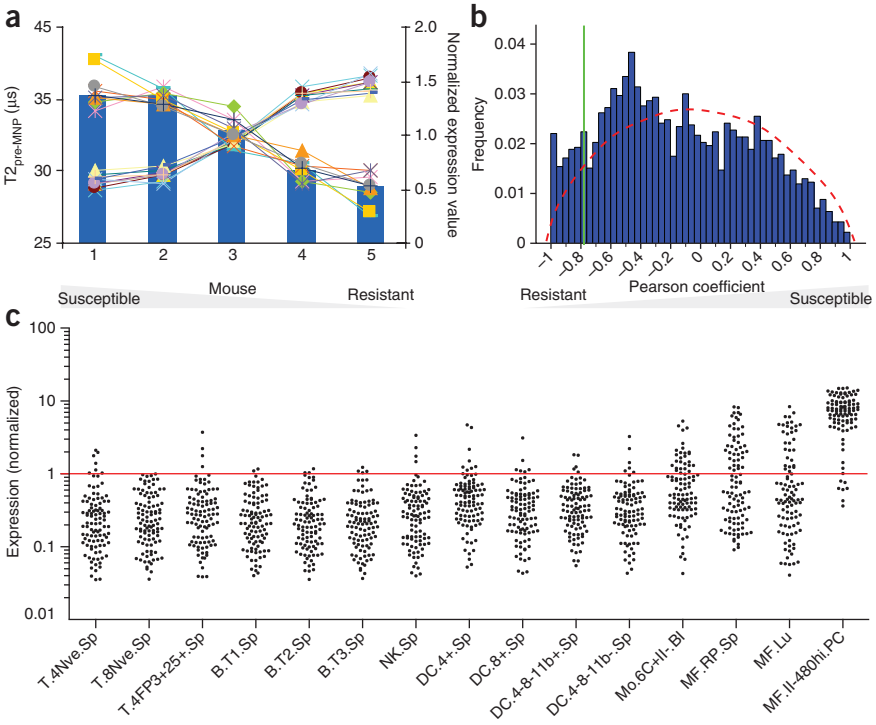

Figure 3 Gene-expression profiling of pancreas-resident hematopoietic cells as a function of MRI signal. Gene expression of purified $CD45^+$ cells from the pancreas of 10-week-old female NOD mice ($n = 5$; horizontal axis) given MRI scans; gene-expression values are correlated to the T2 values. (**a**) Normalized expression profiles of genes whose expression most positively or negatively correlated with T2 values (each line represents an individual gene), superimposed on T2 values before injection of MNPs (blue bars). (**b**) Distribution of the correlation coefficients between expression for all genes and T2 values (blue bars); red dashed line shows the distribution of correlation coefficients in a randomized data set; green line demarcates the 100 genes (left of line) with the most negative correlation, selected for further analysis. (**c**) Cell type–distribution analysis of normalized expression values of the 100 genes selected in **b** (data from the Immunological Genome Project database)[34]. T.4Nve.Sp, naive $CD4^+$ T cells from the spleen; T.8Nve.Sp, naive $CD8^+$ T cells from the spleen; T.4FP3+25+.Sp, natural regulatory T cells from the spleen; B.T1.Sp, B.T2.Sp, B.T3.Sp, transitional B cells (stages 1–3) from the spleen; NK, natural killer cells; DC.4+.Sp, $CD4^+$ DCs from the spleen; DC.8+.Sp, $CD8^+$ DCs from the spleen; DC.4-8-11b+.Sp, $CD4^-CD8^-CD11b^+$ DCs from the spleen; DC.4-8-11b-.Sp, $CD4^-CD8^-CD11b^-$DCs from the spleen; Mo.6C+II-.BI, $Ly6C^+$ monocytes from the blood, negative for major histocompatibility complex class II; MF.RP.Sp, macrophages from the red pulp of the spleen; MF.Lu, macrophages from the lung; MF.II-480hi.PC, $F4/80^{hi}$ peritoneal macrophages negative for major histocompatibility complex class II. Each symbol represents an individual gene; red line indicates normalized mean for all data. Data are representative of two experiments.

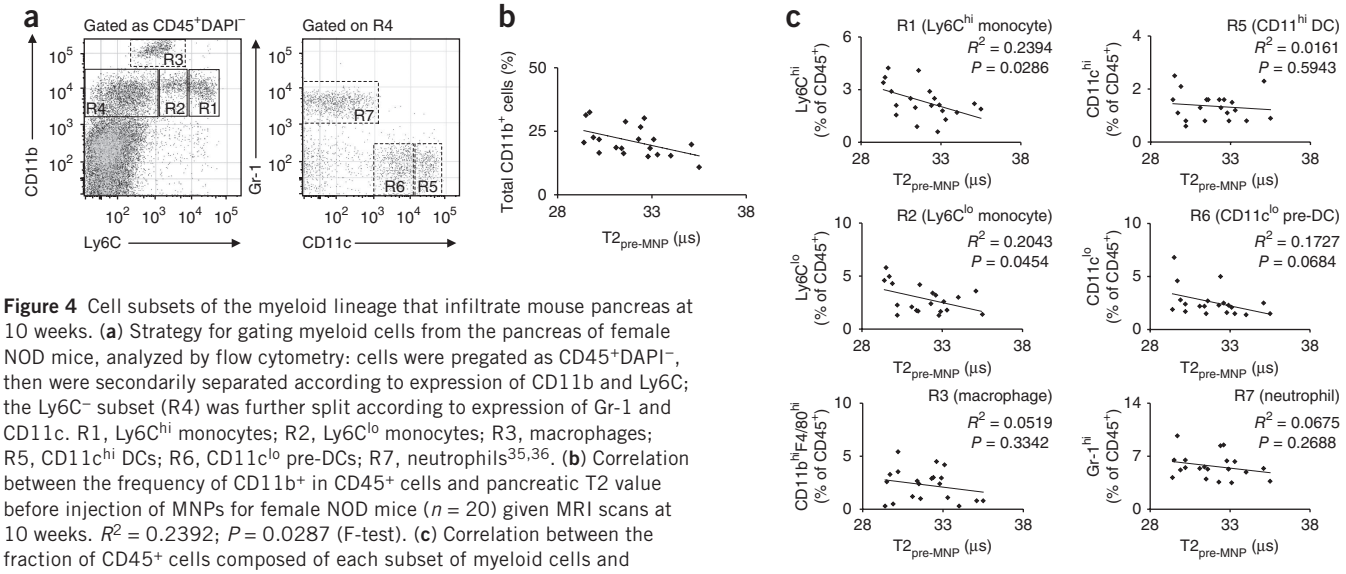

Figure 4 Cell subsets of the myeloid lineage that infiltrate mouse pancreas at 10 weeks. (**a**) Strategy for gating myeloid cells from the pancreas of female NOD mice, analyzed by flow cytometry: cells were pregated as $CD45^+DAPI^-$, then were secondarily separated according to expression of CD11b and Ly6C; the $Ly6C^-$ subset (R4) was further split according to expression of Gr-1 and CD11c. R1, $Ly6C^{hi}$ monocytes; R2, $Ly6C^{lo}$ monocytes; R3, macrophages; R5, $CD11c^{hi}$ DCs; R6, $CD11c^{lo}$ pre-DCs; R7, neutrophils[35,36]. (**b**) Correlation between the frequency of $CD11b^+$ in $CD45^+$ cells and pancreatic T2 value before injection of MNPs for female NOD mice ($n = 20$) given MRI scans at 10 weeks. $R^2 = 0.2392$; $P = 0.0287$ (F-test). (**c**) Correlation between the fraction of $CD45^+$ cells composed of each subset of myeloid cells and pancreatic T2 value before injection of MNPs, for the mice in **b**. The R1–R3 and R5–R7 populations are those outlined in **a**. *P* values, F test. Each symbol (**b**,**c**) represents an individual mouse. Data are representative of five experiments (**a**) or are combined from four experiments (**b**,**c**).

the higher imaging signals at 3 weeks dropped quickly, as soon as 6–7 weeks, and remained low thereafter. We noted the same pattern in a group of male NOD mice, which universally manifest insulitis, although very few develop diabetes (**Supplementary Fig. 2b**). We compared the ability of this MRI-MNP procedure and a published assay of autoantibodies to insulin[16] to predict the conversion of insulitis to diabetes in a cohort of NOD mice. Although the number of mice examined was not large, the MRI-MNP approach showed higher significance in terms of the prediction of both eventual diabetes development and time to diabetes (**Fig. 2d**,**e**).

Thus, the MRI-MNP method was able to distinguish, months before clinical manifestation, mice that progressed to diabetes from those that did not, and also allowed an estimation of the time to diabetes onset. One implication of these findings is that eventual conversion of insulitis to diabetes is set at a young age. In addition, it is now possible to explore in an accurate manner what molecular and cellular processes underlie this conversion.

Overexpression of myeloid lineage–associated genes

To exploit the new possibilities offered by the ability to select a given 6- to 10-week-old NOD mouse and predict with quite good accuracy whether or not it will go on to develop diabetes, we first followed an unbiased, hypothesis-generating approach, doing microarray-based gene-expression profiling of pancreas-residing leukocytes from prediabetic and nondiabetic mice. We scanned cohorts of five female mice by MRI at 10 weeks of age, removed their pancreata immediately after the final imaging and sorted $CD45^+$ cells from the dispersed tissue for microarray analysis of gene expression. We were interested in genes whose transcripts were positively or negatively correlated with the MRI signals, as they might promote diabetes or protect from diabetes, respectively. We calculated the Pearson correlation coefficient for the normalized expression value of each gene and the T2 signals before injection of MNPs for the five mice. As an illustration, we superimposed the expression profiles for the ten genes with the greatest positive or negative correlation onto the histogram of T2 values (**Fig. 3a**). Overall, the correlation coefficients of all genes on the microarray were distributed across the spectrum but with a bias for those whose transcription negatively correlated with T2 signals relative to the null-hypothesis distribution of a randomized permutation of the expression data (**Fig. 3b**). This bias was particularly marked for those transcripts that had the lowest correlation coefficients (≤−0.8) and thus were associated with resistance to diabetes, in contrast to published studies of aggressive diabetes in which the dominant signatures were those associated with inflammation[17]. Therefore, we focused our subsequent analyses on the 100 'protective' genes with the greatest negative correlation (**Supplementary Table 1**).

Changes in transcript abundance in the $CD45^+$ cell populations of the various mice could have reflected alterations in the composition of the leukocytic infiltrate and/or modifications in gene-expression programs. To address this issue by bioinformatics, we generated a cell-distribution profile, plotting for each of the 100 genes its normalized expression in a panel of cell types, using data sets available from the Immunological Genome Project (**Fig. 3c**). The set of genes whose transcript abundance was negatively correlated with the T2 values before injection of MNPs were characteristic of cells of the myeloid lineage, in particular, tissue-resident macrophages.

The over-representation of genes characteristic of cells of the myeloid lineage prompted us to explore the cellular composition of the insulitic lesion by histology and flow cytometry of 10-week-old female NOD mice scanned by MRI (**Fig. 4** and **Supplementary Fig. 3**). In the mice with lower MRI signals (those predicted to be refractory to diabetes), insulitis was less extensive (**Supplementary Fig. 3a**) and fewer leukocytes infiltrated the pancreas (**Supplementary Fig. 3b**), largely due to a lower abundance of $CD3^+$ T cells (**Supplementary Fig. 3b**). There were no other obvious differences in the histological presentation of the insulitic lesions at this age (**Supplementary Fig. 3b** and data not shown).

Multiparameter flow cytometry of myeloid cell populations did yield some clear associations with MRI signals. Our gating strategy (**Fig. 4a**) distinguished among the main $CD11b^+$ myeloid cell populations: two subsets of monocytes ($Ly6C^{hi}$ (R1 gate) and $Ly6C^{lo}$ (R2 gate)), mature macrophages (R3 gate), two DC subsets ($CD11c^{hi}$ (R5 gate) and $CD11c^{lo}$ (R6 gate)) and neutrophils (R7 gate). Of note, F4/80, a marker for mature macrophages, was detectable only on cells in the R3 gate (**Supplementary Fig. 4**). The available antibody to the monocyte marker Gr-1, RB6-8C5, detects only Ly6G on neutrophils

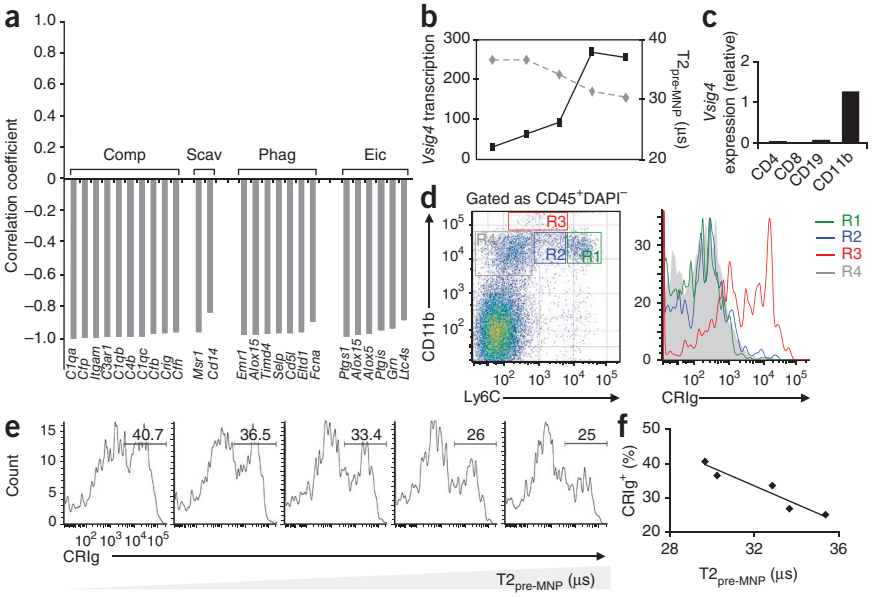

Figure 5 Enrichment for CRIg$^+$ tissue macrophages in pancreas of NOD mice protected from diabetes. (**a**) Correlation coefficient between transcript abundance and pancreatic T2 signal before injection of MNPs, grouped into distinct functional classes for genes encoding molecules associated with diabetes protection (strong anticorrelation with pancreatic T2 values): Comp, complement-pathway components; Scav, scavenger receptors; Phag, phagocytosis-related proteins; Eic, eicosanoids. (**b**) Correlation between pancreatic T2 values before injection of MNPs (dashed line) and abundance of transcripts encoding CRIg (*Vsig4*; solid line), determined from the same microarray data set as in **Figure 3**. Transcript results are presented relative to those of *Hprt1* (encoding hypoxanthine guanine phosphoribosyl transferase). (**c**) Quantitative RT-PCR analysis of expression of the gene encoding CRIg (*Vsig4*) in various cell types isolated from the pancreas of 10-week-old NOD mice; results are presented relative to those of *Hprt1*. (**d**) CRIg expression on pancreatic cells of the myeloid lineage from 10-week-old NOD mice. R1–R4 correspond to the regions gated at left. (**e**) Frequency of CRIg$^+$ macrophages in pancreatic lesions in a cohort of 10-week-old female NOD mice (independent of those used for **Fig. 4**), and T2 signal before injection of MNPs (wedge, below). Numbers above bracketed lines indicate percent CRIg$^+$ cells in the CD45$^+$DAPI$^-$CD11b$^+$F4/80$^+$ gate (macrophages), set by comparison with an isotype-matched control monoclonal antibody. (**f**) Correlation between MRI signals and frequency of CRIg$^+$ macrophages in the pancreas for the cohort in **e**. $R^2 = 0.9212$; $P = 0.0096$ (F-test). Data are representative of two experiments (**a**), three experiments (**b**–**d**) or one experiment with five mice (**e**,**f**).

from mice of the NOD strain, in contrast to its ability to additionally detect Ly6C on the monocyte populations from mice of other strains (data not shown). From a general perspective, there was a negative correlation between total pancreatic myeloid cells (CD11b$^+$) and MRI values (**Fig. 4b**); the larger fraction of CD11b$^+$ cells in mice refractory to diabetes was accompanied by a smaller fraction of T cells (CD3$^+$) (**Supplementary Fig. 3c**). More specifically, the pancreatic infiltrates of all mice included several myeloid cell populations: in most cases, there was no evident correlation between their representation and MRI values; however, the fraction of Ly6C^{hi} CD11b$^+$ monocytes and of Ly6C^{lo} CD11b$^+$ monocytes showed a significant negative correlation with T2 values before injection of MNPs (**Fig. 4c**), which indicated enrichment of these subsets in diabetes-resistant NOD mice. Thus, the data from gene-expression and cell-subset profiling converged to highlight greater numbers and/or function of certain subsets of myeloid-lineage cells in 10-week-old NOD mice that showed insulitis but were refractory to clinical diabetes.

Macrophages that express the complement receptor CRIg

Pathway analysis of the subset of genes whose expression had the greatest negative correlation with baseline T2 values (that is, those best correlated with diabetes resistance) showed enrichment for several functional classes characteristic of the monocyte-macrophage lineage: components of the complement pathway, scavenger receptors, phagocytosis-related proteins and eicosanoids (**Fig. 5a**). Our attention was drawn in particular to the complement-pathway component CRIg because it is expressed exclusively on tissue-resident macrophages[18–22], it is reported to inhibit the activation, proliferation and cytokine production of T cells[19,23,24], and fusions of CRIg and the Fc portion of immunoglobulin can modulate autoimmune and inflammatory diseases[24–26]. The abundance of transcripts encoding CRIg in pancreatic CD45$^+$ cells showed a strong negative correlation with T2 signals before injection of MNPs (**Fig. 5b**). CRIg transcripts were most abundant in CD11b$^+$ cells of the myeloid lineage (**Fig. 5c**), and CRIg protein was displayed on a population of fully mature macrophages (**Fig. 5d**), which could best be distinguished as CD11b^{hi}F4/80^{hi} (**Supplementary Fig. 4**). As a whole, the mature macrophage subset in the pancreatic infiltrate showed no correlation, positive or negative, with MRI signals (**Fig. 4c**); however, analysis of another cohort of mice showed a strong negative correlation between baseline T2 values and the fraction of CD11b$^+$F4/80$^+$ mature macrophages that were CRIg$^+$ (**Fig. 5e**,**f**). We also detected CRIg$^+$F4/80$^+$ cells histologically, located mainly at the periphery of the insulitic lesion (**Supplementary Fig. 5a**), often in close association with CD31$^+$ vascular endothelial cells (**Supplementary Fig. 5b**). CRIg$^+$ macrophages were also present in the pancreas of Eα16/NOD mice (**Supplementary Fig. 6**), which are completely free of insulitis and diabetes[15]; this result reflected the normal tissue residence of CRIg$^+$ macrophages, as has been observed in several other contexts[18,20,22]. Hence, in young NOD mice, MRI-MNP signals (a biomarker of diabetes development) can be used to identify potential candidate molecules, pathways or cells associated with disease protection.

CRIg modulates MRI signals and diabetes

Next we explored whether the anticorrelation of pancreatic CRIg expression and MRI signals in juvenile NOD mice has functional relevance. First, we verified that a CRIg-Fc fusion protein suppressed the proliferation of NOD T cells during culture *in vitro*, in a dose-dependent manner (**Supplementary Fig. 7**), as has been reported in other contexts for other mouse strains[19,23,24]. To determine whether CRIg expression by pancreas-resident macrophages might have a causal relationship with MRI signal intensity and eventual diabetes development, we injected either CRIg-Fc or a control Fc fusion protein into cohorts of female NOD mice from 3 to 10 weeks of age, an interval that spans the initiation and establishment of insulitis.

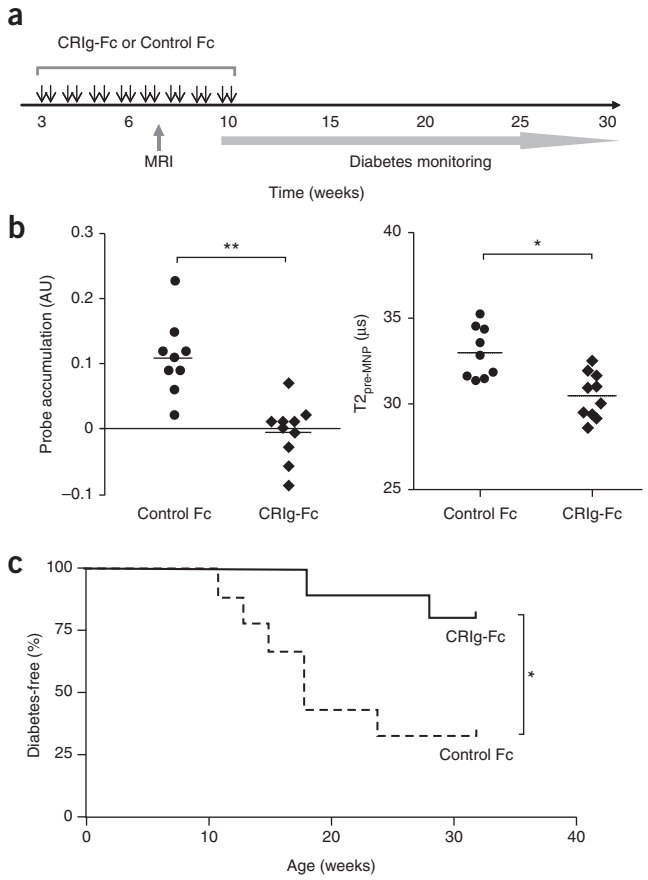

Figure 6 Inhibition of pancreatic MRI-MNP signals and protection from diabetes after treatment of NOD female mice with CRIg-Fc. (**a**) Experimental design: 3-week-old female NOD mice were injected intraperitoneally with CRIg-Fc or a control Fc fusion protein (Control Fc) twice a week until 10 weeks of age and given MRI-MNP screening at 7–8 weeks, then were monitored for diabetes development until 32 weeks of age. (**b**) Probe accumulation (left) and pancreatic T2 values before injection of MNPs (right) in mice given CRIg-Fc ($n = 10$) or the control Fc fusion protein ($n = 9$). Each symbol represents an individual mouse; small horizontal lines indicate the mean. $^{*}P = 0.0012$ and $^{**}P = 0.0001$ (Student's *t*-test). (**c**) Diabetes development in the mice in **b**. $^{*}P = 0.0196$ (Gehan-Breslow-Wilcoxon test). Data are combined from two experiments with 19 mice.

We scanned the mice by MRI at 7–8 weeks of age (the predictive window) and monitored diabetes development from 10 to 32 weeks (**Fig. 6a**). As expected, the range of probe-accumulation values for mice given the control Fc fusion protein spanned values typical of nondiabetic mice (−0.05 to 0.05) and prediabetic mice (0–0.33) at that age (**Fig. 6b**, left). In clear contrast, the corresponding values for mice given CRIg-Fc protein were almost all within the lower range expected of nondiabetic mice (**Fig. 6b**, left). There was also a significant difference between mice treated with CRIg-Fc and those treated with control Fc fusion protein for T2 values before injection of MNPs (**Fig. 6b**, right). As would be predicted from such a lowering of MRI signals, diabetes development was significantly delayed and less frequent (20% versus 67%) in mice that had been injected with CRIg-Fc compared with its development in those treated with control Fc fusion protein (**Fig. 6c**). Therefore, CRIg itself and $CRIg^{+}$ macrophages can be considered additional participants in the pathogenesis of type 1 diabetes, as protective elements whose enhancement has potential therapeutic benefit.

DISCUSSION

The MRI-MNP procedure can be used to monitor the development of diabetes in NOD mice, to quantify genetically determined variability in disease severity in derivative models, to predict the imminent onset of clinical diabetes and to monitor disease reversal subsequent to immunotherapy[6,7]. This approach has also been 'translated' to humans to successfully discriminate normal controls from patients recently diagnosed with type 1 diabetes, which has opened the door to noninvasive monitoring of response to immunotherapy in clinical trials[12]. Here we focused on optimizing the MRI-MNP approach as a prediction tool in the NOD model. The most notable finding was that MRI signals (T2 values before injection of MNPs and, even better, probe-accumulation values) measured during a discrete, early time window distinguished between mice that would or would not go on to develop clinical diabetes and permitted an estimation of time to onset of diabetes. This observation has theoretical and practical ramifications.

First, the finding that whether or not a given NOD mouse will eventually develop overt diabetes is already set at 6–10 weeks of age has implications for the reigning theories of the pathogenesis of type 1 diabetes, at least for the NOD mouse model. Scenarios that require a 'second hit' for progression from insulitis to diabetes, such as some microbial, dietary or stress-related insult, seem to be inconsistent with such an early window of determinism. Scenarios that call for delayed stochastic generation of the ultimately pathogenic T cell or B cell specificities would also seem to be disfavored. Instead, our findings indicate that some early event that occurs before 6 weeks of age predicates the development of clinical diabetes in a fraction of the NOD mouse colony but that regulatory processes keep the insulitic lesion in check for variable lengths of time in different mice. That conclusion is consistent with a report that early development of autoantibodies to insulin could be used to predict eventual diabetes development in NOD mice[16], although results from subsequent studies have not seemed to support the generality of that finding[27].

The practical implication of the MRI-MNP data is that individual young NOD mice can now be sorted into groups that should or should not progress to clinical type 1 diabetes. In addition to permitting more meaningful interpretation of results from diabetes-prevention trials, this ability allows pathogenetic mechanisms to be addressed in a much more accurate manner. Mechanistic dissections of the NOD model have always been compromised by the heterogeneity in disease penetrance and kinetics; MNP-MRI signals will allow the correlation of chosen experimental parameters with the likelihood and proximity of diabetes onset. Although the fairly high cost of this technique at present precludes high-throughput use, we anticipate that the price will decrease in time, as is often seen with sophisticated technologies like this. Exploiting this approach, we were able to identify in the islet infiltrates of 10-week-old NOD mice specific cells and molecules whose representation was correlated with protection from clinical diabetes.

Both the molecular analyses and cellular analyses indicated a role for cells of the myeloid lineage in disease attenuation. The set of loci whose expression in islet-infiltrating leukocytes had the strongest negative correlation with MRI signals (that is, high expression reflected a low probability of progression to diabetes) showed considerable enrichment for genes expressed by monocytes and macrophages, in particular, tissue-resident macrophages. Similarly, the only cell types with a significant negative correlation with MRI signals were $Ly6C^{hi}$ monocytes, $Ly6C^{lo}$ monocytes and $CRIg^{+}$ tissue-resident macrophages. A regulatory role for cells of the myeloid lineage would be consistent with the growing number of this lineage's members

recognized as having immunosuppressive activity[28,29]. As for the diabetes context, macrophages are the earliest detectable hematopoietic cells in the islets of NOD mice and certain other models of type 1 diabetes[11], and it has been generally assumed that they promote insulitis and its progression to diabetes. However, it is not known at present which particular subsets of monocytes-macrophages participate in the insulitic lesion, at what specific disease stages they do so and whether they have a positive or negative role in diabetes progression.

Of the set of transcripts showing enrichment in the islet infiltrates of mice that did not progress to diabetes, we were particularly intrigued by those encoding CRIg because this molecule is expressed exclusively by tissue-resident macrophages[18–22], it inhibits the activation, proliferation and cytokine production of T cells[19,23,24], and reagents derived from CRIg modulate autoimmune and inflammatory diseases, notably experimental arthritis and uveitis[24–26]. Indeed, CRIg proved relevant in the present context: it marked a specific subset of macrophages whose representation in the insulitic infiltrate showed a significant negative correlation with MRI values at 10 weeks and, most notably, administration of a CRIg-Fc fusion protein both lowered the MRI values and inhibited development of type 1 diabetes. How might CRIg$^+$ macrophages, CRIg itself and CRIg-Fc act to control the progression to overt diabetes? So far, CRIg has been ascribed the following three functions[30]: it acts in the phagocytosis of particles, microbes and cells, via binding to C3b and iC3b; it inhibits the alternative pathway of complement, through blockade of the C3 and C5 convertases; and it suppresses T cells, which reflects its membership in the B7 family of costimulatory or coinhibitory receptors. The proposal that CRIg's function as a negative regulator of T cell activation is important in the diabetes context is supported by the finding of a smaller fraction of CD3$^+$ T cells in the insulitic lesions of NOD mice that did not progress to diabetes. According to such a scenario, CRIg-Fc would deliver a negative signal directly to T cells. CRIg, as a B7 homolog, is expressed by antigen-presenting cells, not T cells. Thus, CRIg-Fc would not be expected to block interactions between antigen-presenting cells and T cells as, for example, a fusion of the immunomodulatory receptor CTLA-4 (found on T cells) and immunoglobulin does; instead, CRIg would be expected to engage an as-yet-unidentified ligand on T cells, just as a fusion of the ligand for the costimulatory molecule PD-1 and immunoglobulin delivers a negative signal directly to T cells by engaging PD-1 (ref. 31). Indeed, CRIg-Fc has been found to directly inhibit T cell proliferation in an *in vitro* assay[19].

It is also possible that CRIg's activity in promoting phagocytosis has a role in keeping diabetes in check in unmanipulated NOD mice. Effective clearance of apoptotic cells, whether engendered by the wave of physiological beta-cell death known to take place at 3 weeks of age in rodents[32] or by some microbial, dietary or stress-inducing insult, could promote tolerance rather than immunity. Of note, the set of transcripts negatively correlated with diabetes development included many that encode proteins involved in opsonization or phagocytosis. For example, MSR1 and CD14 enable tissue-resident macrophages to clear apoptotic cells and dampen inflammation. In addition, transcripts encoding Timd4, a phosphatidylserine receptor[33], were upregulated in diabetes-resistant mice. CRIg$^+$ macrophages also had high expression of Timd4, which suggests a potential molecular basis for the recognition of apoptotic cells by CRIg$^+$ macrophages. Disease inhibition would be reinforced by local dampening of pathogenic T lymphocyte reactivity to beta cells, as discussed above.

Thus, the studies described here have provided proof of the principle that the ability to distinguish closely matched NOD mice that progress or do not progress to diabetes can yield new mechanistic insights. This new information may suggest new therapeutic approaches. A next step will be to apply the MRI-MNP approach to at-risk humans to determine whether it can be used as a tool to predict type 1 diabetes.

METHODS

Methods and any associated references are available in the online version of the paper at http://www.nature.com/natureimmunology/.

Accession codes. GEO: microarray data, GSE35096.

Note: Supplementary information is available on the Nature Immunology website.

ACKNOWLEDGMENTS

We thank M. van Lookeren Campagne (Genentech) for discussions and for monoclonal antibody to CRIg and the CRIg-Fc fusion protein; G. Eisenbarth and L. Yu for measuring autoantibodies to insulin; U. Mahmood and A. Guimaraes for MRI protocol setup and discussions; C. Kaufman and J. Chan for assistance with MRI; J. Pagan, K. Hattori, P. Waterman and A. Sumski for assistance with mice; J. Hill, K. Leatherbee, M. Painter and S. Davis for microarray experimentation and analysis; J. Nishio for histology and diabetes monitoring; and J. LaVecchio and G. Buruzala for help with flow cytometry. Supported by the US National Institutes of Health (P01 AI054904 to D.M., C.B. and R.W.), the core facilities of the Joslin Diabetes Center (P30 DK036836), the Manipulated NOD Mouse Core of the Juvenile Diabetes Research Foundation Center on Immunological Tolerance at Harvard Medical School (4-2007-1057), the Mouse Imaging Resource at the Massachusetts General Hospital (U24CA092782) and the American Diabetes Association (7-07-BETA-14 to W.F.).

AUTHOR CONTRIBUTIONS

W.F., R.W., C.B. and D.M. designed experiments; W.F. and G.W. did experiments; all authors analyzed the data; and W.F., R.W., C.B. and D.M. wrote the manuscript.

COMPETING FINANCIAL INTERESTS

The authors declare no competing financial interests.

Published online at http://www.nature.com/natureimmunology/.
Reprints and permissions information is available online at http://www.nature.com/reprints/index.html.

1. Bluestone, J.A., Herold, K. & Eisenbarth, G. Genetics, pathogenesis and clinical interventions in type 1 diabetes. *Nature* **464**, 1293–1300 (2010).
2. André-Schmutz, I., Hindelang, C., Benoist, C. & Mathis, D. Cellular and molecular changes accompanying the progression from insulitis to diabetes. *Eur. J. Immunol.* **29**, 245–255 (1999).
3. Orban, T. *et al.* Pancreatic islet autoantibodies as predictors of type 1 diabetes in the Diabetes Prevention Trial-Type 1. *Diabetes Care* **32**, 2269–2274 (2009).
4. Polonsky, K.S. & Rubenstein, A.H. C-peptide as a measure of the secretion and hepatic extraction of insulin. Pitfalls and limitations. *Diabetes* **33**, 486–494 (1984).
5. Mathis, D. & Gaglia, J. in *Molecular Imaging* (eds. Weissleder R., Ross, B.D., Rehemtulla, A. & Gambhir, S.S.) 1130–1146 (People's Medical Publishing House-USA, Shelton, Connecticut, 2010).
6. Denis, M.C., Mahmood, U., Benoist, C., Mathis, D. & Weissleder, R. Imaging inflammation of the pancreatic islets in type 1 diabetes. *Proc. Natl. Acad. Sci. USA* **101**, 12634–12639 (2004).
7. Turvey, S.E. *et al.* Noninvasive imaging of pancreatic inflammation and its reversal in type 1 diabetes. *J. Clin. Invest.* **115**, 2454–2461 (2005).
8. Papaccio, G., Latronico, M.V., Pisanti, F.A., Federlin, K. & Linn, T. Adhesion molecules and microvascular changes in the nonobese diabetic (NOD) mouse pancreas. An NO-inhibitor (L-NAME) is unable to block adhesion inflammation-induced activation. *Autoimmunity* **27**, 65–77 (1998).
9. Papaccio, G., Pisanti, F.A., Di Montefiano, R., Graziano, A. & Latronico, M.V.G. Th1 and Th2 cytokines exert regulatory effects upon islet microvascular areas in the NOD mouse. *J. Cell Biochem.* **86**, 651–664 (2002).
10. Carlsson, P.O., Sandler, S. & Jansson, L. Pancreatic islet blood perfusion in the nonobese diabetic mouse: diabetes-prone female mice exhibit a higher blood flow compared with male mice in the prediabetic phase. *Endocrinology* **139**, 3534–3541 (1998).
11. Jansen, A. *et al.* Immunohistochemical characterization of monocytes-macrophages and dendritic cells involved in the initiation of the insulitis and beta-cell destruction in NOD mice. *Diabetes* **43**, 667–675 (1994).
12. Gaglia, J.L. *et al.* Noninvasive imaging of pancreatic islet inflammation in type 1A diabetes patients. *J. Clin. Invest.* **121**, 442–445 (2011).
13. Weissleder, R. *et al.* MR lymphography: study of a high-efficiency lymphotrophic agent. *Radiology* **191**, 225–230 (1994).

14. Mills, A.N. & Haworth, S.G. Greater permeability of the neonatal lung. Postnatal changes in surface charge and biochemistry of porcine pulmonary capillary endothelium. *J. Thorac. Cardiovasc. Surg.* **101**, 909–916 (1991).
15. Böhme, J., Schuhbaur, B., Kanagawa, O., Benoist, C. & Mathis, D. MHC-linked protection from diabetes dissociated from clonal deletion of T cells. *Science* **249**, 293–295 (1990).
16. Yu, L. *et al.* Early expression of antiinsulin autoantibodies of humans and the NOD mouse: evidence for early determination of subsequent diabetes. *Proc. Natl. Acad. Sci. USA* **97**, 1701–1706 (2000).
17. Poirot, L., Benoist, C. & Mathis, D. Natural killer cells distinguish innocuous and destructive forms of pancreatic islet autoimmunity. *Proc. Natl. Acad. Sci. USA* **101**, 8102–8107 (2004).
18. Helmy, K.Y. *et al.* CRIg: a macrophage complement receptor required for phagocytosis of circulating pathogens. *Cell* **124**, 915–927 (2006).
19. Vogt, L. *et al.* VSIG4, a B7 family-related protein, is a negative regulator of T cell activation. *J. Clin. Invest.* **116**, 2817–2826 (2006).
20. Tanaka, M. *et al.* Expansion of a unique macrophage subset in rheumatoid arthritis synovial lining layer. *Clin. Exp. Immunol.* **154**, 38–47 (2008).
21. Guo, S. *et al.* Down-regulation of Z39Ig on macrophages by IFN-γ in patients with chronic HBV infection. *Clin. Immunol.* **136**, 282–291 (2010).
22. Gorgani, N.N. *et al.* Complement receptor of the Ig superfamily enhances complement-mediated phagocytosis in a subpopulation of tissue resident macrophages. *J. Immunol.* **181**, 7902–7908 (2008).
23. Xu, S. *et al.* Induction of T cells suppression by dendritic cells transfected with VSIG4 recombinant adenovirus. *Immunol. Lett.* **128**, 46–50 (2010).
24. Chen, M., Muckersie, E., Luo, C., Forrester, J.V. & Xu, H. Inhibition of the alternative pathway of complement activation reduces inflammation in experimental autoimmune uveoretinitis. *Eur. J. Immunol.* **40**, 2870–2881 (2010).
25. Katschke, K.J. Jr. *et al.* A novel inhibitor of the alternative pathway of complement reverses inflammation and bone destruction in experimental arthritis. *J. Exp. Med.* **204**, 1319–1325 (2007).
26. Chen, J., Crispin, J.C., Dalle, L.J. & Tsokos, G.C. A novel inhibitor of the alternative pathway of complement attenuates intestinal ischemia/reperfusion-induced injury. *J. Surg. Res.* **167**, e131–e136 (2011).
27. Robles, D.T., Eisenbarth, G.S., Dailey, N.J., Peterson, L.B. & Wicker, L.S. Insulin autoantibodies are associated with islet inflammation but not always related to diabetes progression in NOD congenic mice. *Diabetes* **52**, 882–886 (2003).
28. Gabrilovich, D.I. & Nagaraj, S. Myeloid-derived suppressor cells as regulators of the immune system. *Nat. Rev. Immunol.* **9**, 162–174 (2009).
29. Geissmann, F. *et al.* Development of monocytes, macrophages, and dendritic cells. *Science* **327**, 656–661 (2010).
30. He, J.Q., Wiesmann, C. & van Lookeren, C.M. A role of macrophage complement receptor CRIg in immune clearance and inflammation. *Mol. Immunol.* **45**, 4041–4047 (2008).
31. Freeman, G.J. *et al.* Engagement of the PD-1 immunoinhibitory receptor by a novel B7 family member leads to negative regulation of lymphocyte activation. *J. Exp. Med.* **192**, 1027–1034 (2000).
32. Mathis, D., Vence, L. & Benoist, C. beta-Cell death during progression to diabetes. *Nature* **414**, 792–798 (2001).
33. Miyanishi, M. *et al.* Identification of Tim4 as a phosphatidylserine receptor. *Nature* **450**, 435–439 (2007).
34. Heng, T.S. & Painter, M.W. The Immunological Genome Project: networks of gene expression in immune cells. *Nat. Immunol.* **9**, 1091–1094 (2008).
35. Gordon, S. & Taylor, P.R. Monocyte and macrophage heterogeneity. *Nat. Rev. Immunol.* **5**, 953–964 (2005).
36. Swirski, F.K. *et al.* Identification of splenic reservoir monocytes and their deployment to inflammatory sites. *Science* **325**, 612–616 (2009).

ONLINE METHODS

Mice. NOD/Lt, Eα16/NOD and C57BL/6 mice were bred under specific pathogen–free conditions in the animal facility of the Joslin Diabetes Center. They were cared for in accordance with the ethical guidelines of the Joslin Diabetes Center and Harvard Medical School, all studies having been approved by the Institutional Animal Care and Use Committee of Joslin Diabetes Center (99-20). Mice were monitored for diabetes development as described[37]; a mouse with two consecutive measurements of a serum glucose concentration above 350 mg/dl was considered diabetic.

MRI-MNP. The MNP used in these experiments was MION-47, which has a diameter of about 22 nm and an R2 relaxivity of 69 (mM^{-1} sec^{-1}) at 37 °C (0.47 T). Mice were anesthetized by inhalation of isoflurane and were placed in a birdcage radio-frequency coil with an inner diameter of 38 mm. A 4.7-Tesla microimaging system was used (PharmaScan; Bruker BioSpin); the imaging protocol included multiple-slice and multiple-echo spin-echo sequences with 16 different echo times: 8.68, 17.36, 26.04, 34.72, 43.40, 52.08, 60.76, 69.44, 78.12, 86.80, 95.48,104.16, 112.84, 121.52, 130.20 and 138.88 microseconds. Other parameters included the following: repetition time, 2325 microseconds; field of view, 4 × 4; matrix size, 128 × 128; slice thickness, 0.6 mm (interleaved); number of excitations, four. To cover the entire pancreatic region, 16 sequential coronal images were obtained. Before MNP injection, mice were scanned for a baseline T2 value. Without removal of the mouse from the coil, MNPs were injected intravenously at a dose of 20 mg Fe per kg body weight to allow quantification of microvascular changes associated with pancreatic inflammation[7]. A third scan was done 24 h after MNP administration to permit quantification of probe accumulation, a function of microvascular leakage and macrophage uptake. Images were analyzed with Osirix software with 'plug-ins' developed in-house. Regions of interest were defined after scanning for three consecutive slices of the pancreas or muscle tissue. To ensure that there were no volume-averaging effects with adjacent organs on calculated T2 values, the regions of interest were 'propagated' to adjacent slices and were modified as needed so that the windows on the original and adjacent slices contained only the tissue of interest. T2 values for individual organs were calculated by fitting of a standard exponential relaxation model to the data averaged over the entire region of interest on each slice. The quantitative probe accumulation was calculated as follows: $[\ln(T2_{pre-MNP}/T2_{24\ h\ post-MNP})]$(ref. 7), where '$T2_{pre-MNP}$' indicates T2 value before MNP injection and '$T2_{24\ h\ post-MNP}$' indicates T2 value 24 h after MNP injection. Results were analyzed independently by two scorers blinded to sample identity.

Microarray. After MRI of mice, pancreata were collected and digested for 30 min at 37 °C with collagenase IV (1 mg/ml) and DNase I (10 U/ml). Single-cell suspensions were prepared and stained, and $CD45^+$ cells were sorted into 500 µl TRIzol (Invitrogen) for RNA isolation. RNA was amplified in two rounds with MessageAmp aRNA (Ambion) and labeled with biotin (BioArray High Yield RNA Transcription Labeling; Enzo), and the resulting cRNA was hybridized to MoGene 1.0 ST arrays (Affymetrix). Raw data were normalized by the robust multi-array average algorithm implemented in the Expression File Creator module of the GenePattern genomic analysis platform[38]. Pearson correlation to the T2 values was computed with S+ software (TIBCO) for real data sets, and randomized data sets were generated by row-wise shuffling. Ingenuity Pathway Analysis software (Ingenuity Systems) was used for pathway-enrichment analysis.

Histology. Pancreata were removed and fixed in 10% neutral-buffered formalin (Sigma-Aldrich). Paraffin-embedded sections were cut in three-step depth 150 µm apart and were stained with hematoxylin and eosin and insulitis was assigned scores as described[37].

Immunostaining and microscopy. Cryosections of pancreas 6 µm in thickness were cut and fixed with cold acetone. Standard procedures were used for immunostaining. Before the addition of primary monoclonal antibodies, sections were blocked with 5% normal donkey serum (Jackson ImmunoResearch). The following monoclonal antibodies were used in various combinations: antibody to CRIg (anti-CRIg; 17C9; a gift from Genentech), anti-F4/80 (BM8; BioLegend), anti-CD11b (M1/70; BioLegend) and anti-CD31 (MEC13.3; BD Pharmingen). Nuclei were stained with DAPI (4′,6-diamidino-2-phenylindole dihydrochloride). Images were acquired on an Axiovert 200M confocal microscope (Zeiss) with a xenon arc lamp in a Lambda DG-4 wavelength switcher (Sutter Instrument) and were processed with Slidebook imaging software (Intelligent Imaging).

Flow cytometry. Single-cell suspensions of pancreata were prepared as above. All staining began with incubation with monoclonal antibody to FcγR (2.4G2; BD Pharmingen). Antibodies used for subsequent staining were as follows: anti-CD45 (30-F11; BD Pharmingen), anti-Ly6C (Al-21; BD Pharmingen), anti-CD11b (M1/70; BioLegend), anti-CD11c (N418; BioLegend), anti-F4/80 (BM8; BioLegend), anti-Gr-1 (RB6-8C5; BioLegend) and anti-CRIg (17C9, a gift from Genentech). Samples were acquired with an LSR II (BD Bioscience) and data were analyzed with FlowJo software (Tree Star).

T cell–proliferation assay. Spleen naive T cells were sorted as $CD4^+CD45R^-CD8^-CD11b^-CD11c^-CD25^-CD62L^{hi}$ and were labeled by incubation for 20 min at 37 °C at a density of 1×10^6 cells per ml in RPMI-1640 medium with CFSE (10 µmol/l; Molecular Probes), then were washed and resuspended in complete medium (10% FCS, L-glutamine (2 mmol/l) and penicillin-streptomycin in RPMI-1640 medium). Cells were cultured at a density of 5×10^4 cells per well in round-bottomed 96-well plates (Corning).

For T cell activation, beads coated with anti-CD3 and -CD28 (Dynabeads) were added at a bead/cell ratio of 1:1, with the addition of IL-2 (20 U/ml; Proleukin; Chiron). CRIg-Fc (Genentech) or control Fc fusion protein (antibody to glycoprotein gp120 immunoglobulin G1; Genentech) was added into the culture medium at the appropriate final concentration. Proliferation was assessed by analysis of CFSE dilution by flow cytometry. Mean division number was calculated as a proliferation index[39].

***In vivo* effect of CRIg-Fc.** Three-week-old female NOD mice were randomly divided into two groups and were treated intraperitoneally twice a week until 10 weeks of age with CRIg-Fc or control Fc fusion protein (antibody to gp120 immunoglobulin G1) at a dose of 4 mg fusion protein per kg body weight. MRI-MNP was done at 7–8 weeks of age. All mice were monitored to 32 weeks of age or longer for the development diabetes.

Statistical analysis. Tests used for statistical analyses are provided in figure legends (GraphPad software v5.0; Prism). *P* values of 0.05 or less were considered statistically significant.

37. Katz, J.D., Wang, B., Haskins, K., Benoist, C. & Mathis, D. Following a diabetogenic T cell from genesis through pathogenesis. *Cell* **76**, 1089–1100 (1993).
38. Reich, M. *et al.* GenePattern 2.0. *Nat. Genet.* **38**, 500–501 (2006).
39. D'Alise, A.M. *et al.* The defect in T-cell regulation in NOD mice is an effect on the T-cell effectors. *Proc. Natl. Acad. Sci. USA* **105**, 19857–19862 (2008).